

# 8e20 Nue Analysis Update

The Nue Group

May 23, 2011

## 1 Intro

Our goal for the 8e20  $\nu_e$  analysis [1] was to seek out analysis improvements that gave us big leaps in sensitivity with otherwise minimal changes to the analysis. These improvements were 1) a new PID (LEM) and 2) fitting in multiple bins. The previous  $\nu_e$  analyses were rate measurements, i.e. the  $\sin^2(2\theta_{13})$  fit was done based only on the total number of selected  $\nu_e$ -like events. A rate measurement with LEM gave us a 13% improvement in sensitivity over a rate measurement with ANN. Fitting in multiple bins gave a 12% improvement over a rate measurement.

Other aspects of the analysis were not changed for the 8e20 analysis. The preselection cuts, including the 1-8 GeV reconstructed energy selection, were optimized during the 3e20 analysis era. The ND decomposition and near to far extrapolation was done in bins of energy for both the 3e20 and 7e20 analyses. However, it has been shown that the FD prediction doesn't change much even if the extrapolation is not binned in energy [2]. This is because the F/N ratio and the ND data/MC discrepancy are essentially flat in energy (there is a slight shape to the  $\nu_\mu$  CC F/N ratio due to oscillations, but it doesn't have a large effect).

All the binning optimization studies done with the LEM PID are summarized in [3]. This document also outlines how the studies were done. The biggest gain in sensitivity comes from including multiple PID bins in the fit. There is a very slight gain in sensitivity (<1%) going from one energy bin to two, but we felt this wasn't significant enough to pursue. There's no further improvement in sensitivity with more than two energy bins. Based on all this information, we decided to do the fit in three LEM bins (0.6-0.7, 0.7-0.8, >0.8) and one energy bin (the full selected range 1-8 GeV). The near to far extrapolation was done using the same bins, but the ND decomposition fit was done in bins of energy and PID.

## 2 8e20 Box Opening

When the box was opened, the distribution seen in Figure 1 was obtained, with the three LEM fit bins populated as listed in Table 1. The best fit for signal was found to be  $\sin^2(2\theta_{13}) = 0.04633$  at  $\delta_{CP} = 0$ .

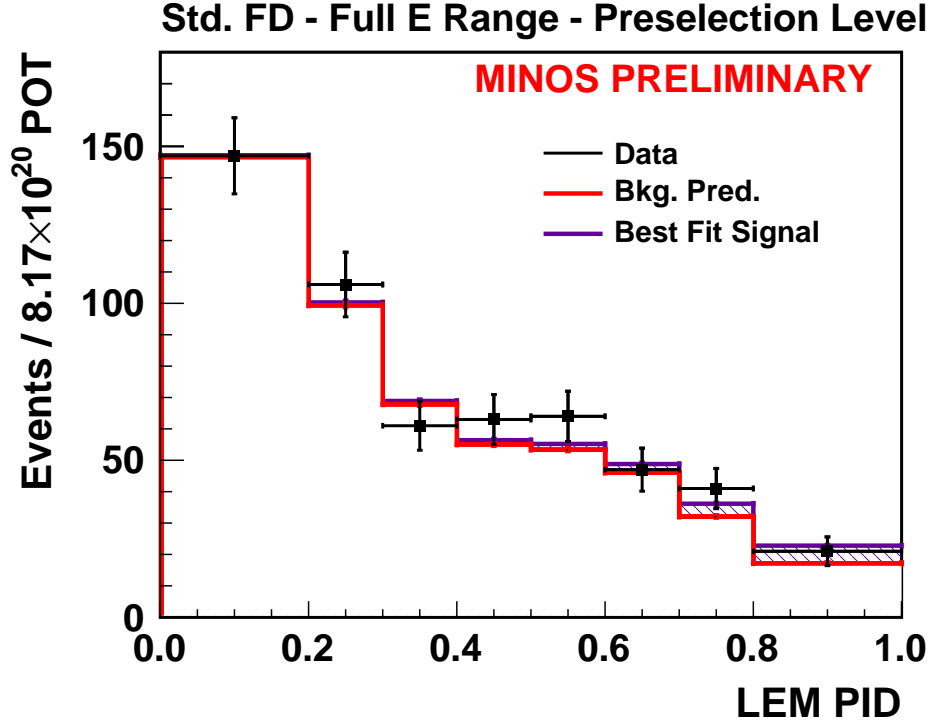


Figure 1: Full LEM particle ID distribution for Background Prediction (red), best fit signal (violet, at  $\sin^2(2\theta_{13}) = 0.04633$ ,  $\delta_{CP} = 0$ ), and Far Data (black). Plot is for all runs and an exposure of  $8.17 \times 10^{20}$  POTs.

	. LEM Bin 1	LEM Bin 2	LEM Bin 3	LEM>0.7	ANN>0.7
Prediction	46.40	32.19	17.46	49.65	57.33
Data	47	41	21	62	65

Table 1: Predictions and Data for the selections

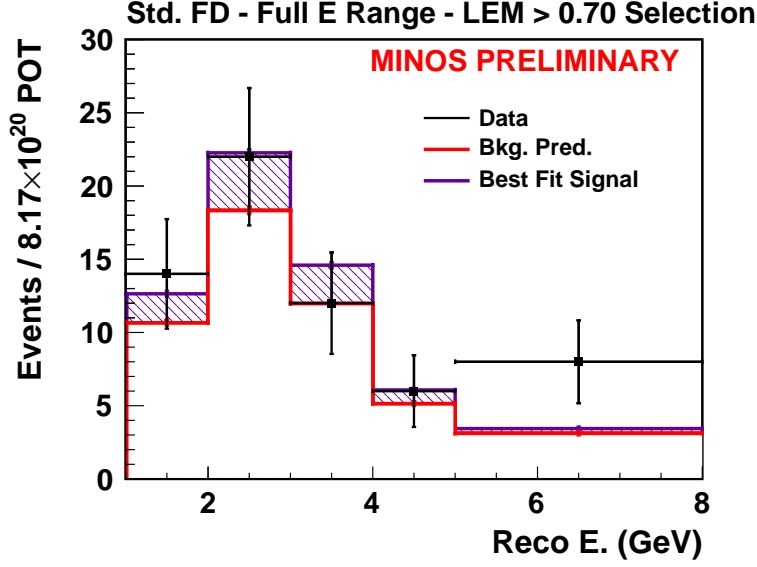


Figure 2: Reconstructed energy distribution for LEM>0.7, for Background Prediction (red), best fit signal (violet, at  $\sin^2(2\theta_{13}) = 0.04633$ ,  $\delta_{CP}=0$ ), and Far Data (black). Plot is for all runs and an exposure of  $8.17 \times 10^{20}$  POTs. The excess in the 5-8 GeV energy bin is striking and triggered the investigation described in this document. Since the energy distribution is not being considered in the fit, the fit tries to compensate for the high energy excess by adding signal, which contributes primarily below 4 GeV.

Several variable distributions comparing the data to the prediction were made to check the result. The first distribution examined was reconstructed energy. The reconstructed energy for LEM>0.70 is shown in Figure 2; the preselection is shown in Figure 3, the individual three LEM bins in Figure 4, and ANN11>0.70 in 5.

The most striking feature of both the Preselection and LEM Selection plots is an excess in the 5-8 GeV energy bin. Since the energy distribution is not being considered, the fit tries to compensate for the high energy excess by adding signal, which contributes primarily below 4 GeV. From the energy distributions of the different LEM regions in Figures 2 and 4, one can see that this best fit signal doesn't make the predicted and observed energy distributions more consistent. In the case of the Preselection, 103.9 events are expected in the 5-8 GeV bin, but 135 are observed. For the case of LEM>0.7, 3.1 events are expected, while 8 are observed in this bin. There is only a slight excess for ANN>0.7, however, with 4.0 events predicted and 5 observed.

For the total 1-8 GeV Preselection reconstructed energy distribution, the agreement between the prediction and data is  $\chi^2=10.3$  (ndof=5), with p=0.0675. For the lower four bins, an agreement is found of  $\chi^2=0.97503$  (ndof=4), for p=0.9136. For the 5-8 GeV bin, however, the disagreement is highly statistically significant, with  $\chi^2=9.31387$  (ndof=1) and

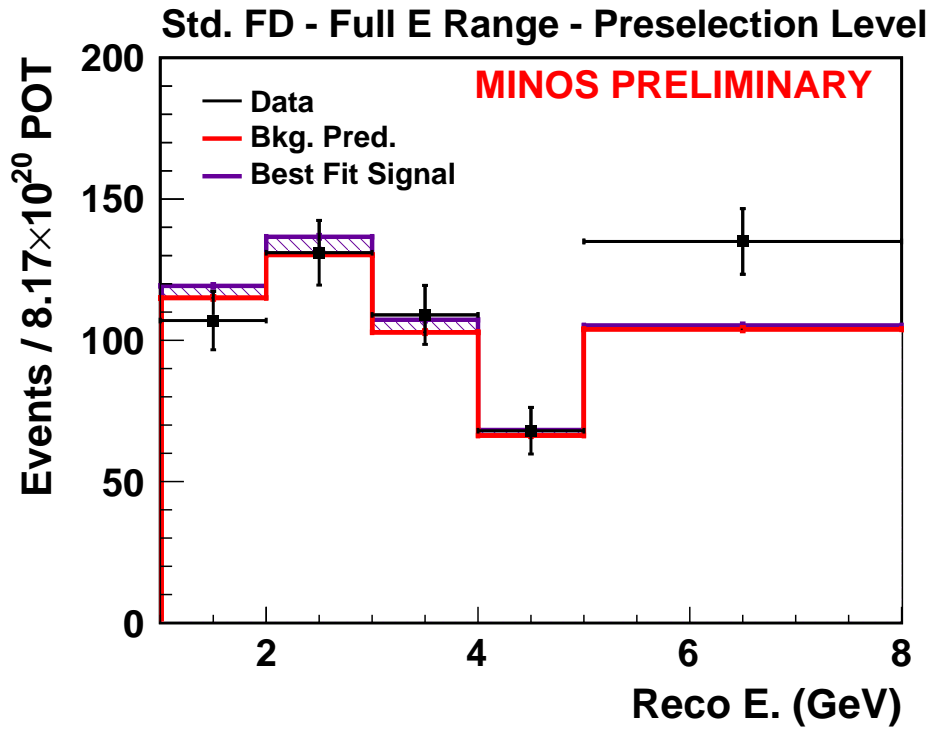


Figure 3: Preselection reconstructed energy distribution, for Background Prediction (red), best fit signal (violet, at  $\sin^2(2\theta_{13}) = 0.04633$ ,  $\delta_{CP}=0$ ), and Far Data (black). Plot is for all runs and an exposure of  $8.17 \times 10^{20}$  POTs.

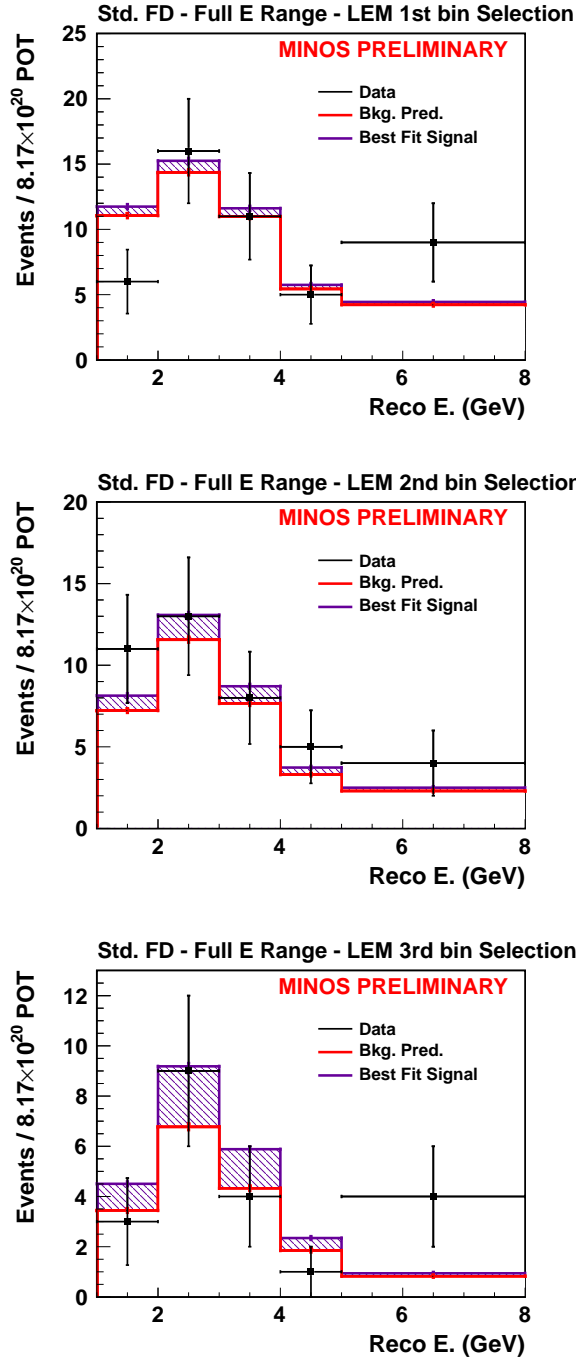


Figure 4: Reconstructed energy distribution for bin 1 ( $0.6 \leq \text{LEM} < 0.7$ , top), bin 2 ( $0.7 \leq \text{LEM} < 0.8$ , middle), and bin 3 ( $0.8 \leq \text{LEM}$ , bottom), for Background Prediction (red), best fit signal (violet, at  $\sin^2(2\theta_{13}) = 0.04633$ ,  $\delta_{CP} = 0$ ), and Far Data (black). Plot is for all runs and an exposure of  $8.17 \times 10^{20}$  POTs.

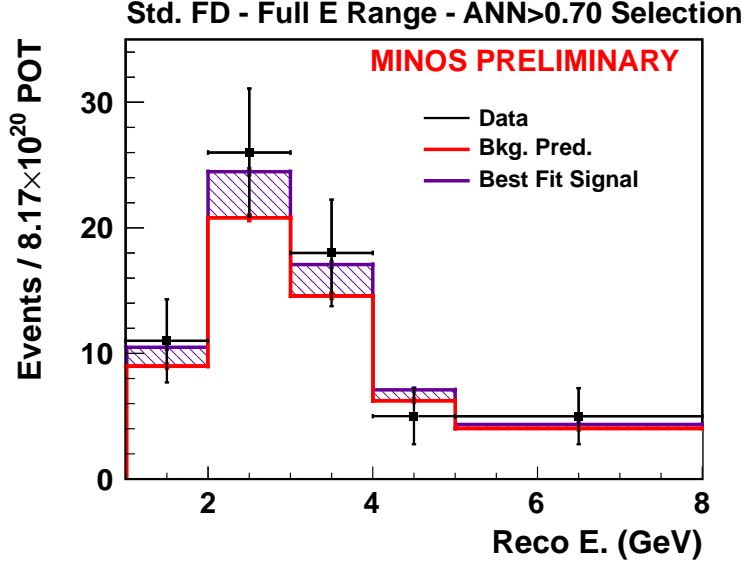


Figure 5: Reconstructed energy distribution for ANN11>0.7, for Background Prediction (red), best fit signal (violet, at  $\sin^2(2\theta_{13}) = 0.04633$ ,  $\delta_{CP}=0$ ), and Far Data (black). Plot is for all runs and an exposure of  $8.17 \times 10^{20}$  POTs.

$p=0.0023$ . The discrepancy between the data and prediction is less statistically significant for LEM>0.70. Unlike the Preselection case, the LEM>0.7 case is in the Poisson statistics regime, and a toy MC study must be performed. For the full 1-8 GeV distribution, 23% of events had a larger value of  $\chi^2$ ; for 1-5 GeV, 78% of events had a larger  $\chi^2$ . For the 5-8 GeV bin, there was a 1.4% chance of there being an excess of eight or more events. Neither of these studies for the Preselection or LEM included systematic error. When these distributions are binned more finely, most of the excess is revealed to be confined to 5-6 GeV. Figure 6 shows the Preselection and LEM>0.70 distribution in bins of 0.5 GeV instead of the standard decomposition binning. 7 of the 8 LEM-selected events in the excess region are in the 5-6 GeV range (additionally, 5 of these in the 5.5-6.0 GeV range). Interestingly, while the largest excess for LEM occurs in 5.5-6 GeV, the largest excess for the preselection is in 5.0-5.5 GeV.

If the extrapolation is performed with 5 decomposition energy bins, instead of one, the size of the excess in the final bin is reduced somewhat for both the Preselection and the LEM selection. In this case,  $109 \pm 10.4$  stat  $\pm 3.6$  syst events are predicted in the 5-8 GeV region for the preselection sample (versus 135 observed events), and  $3.3 \pm 1.8$  stat  $\pm 0.4$  syst events in the LEM>0.70 sample (versus 8 data events). For these numbers, the data exhibits a 2.4 sigma excess for the Preselection, and a <2 sigma excess for LEM. Notably, if one plots the reconstructed energy separately in the three analysis Runs (Figure 7), the excess is present in each Run.

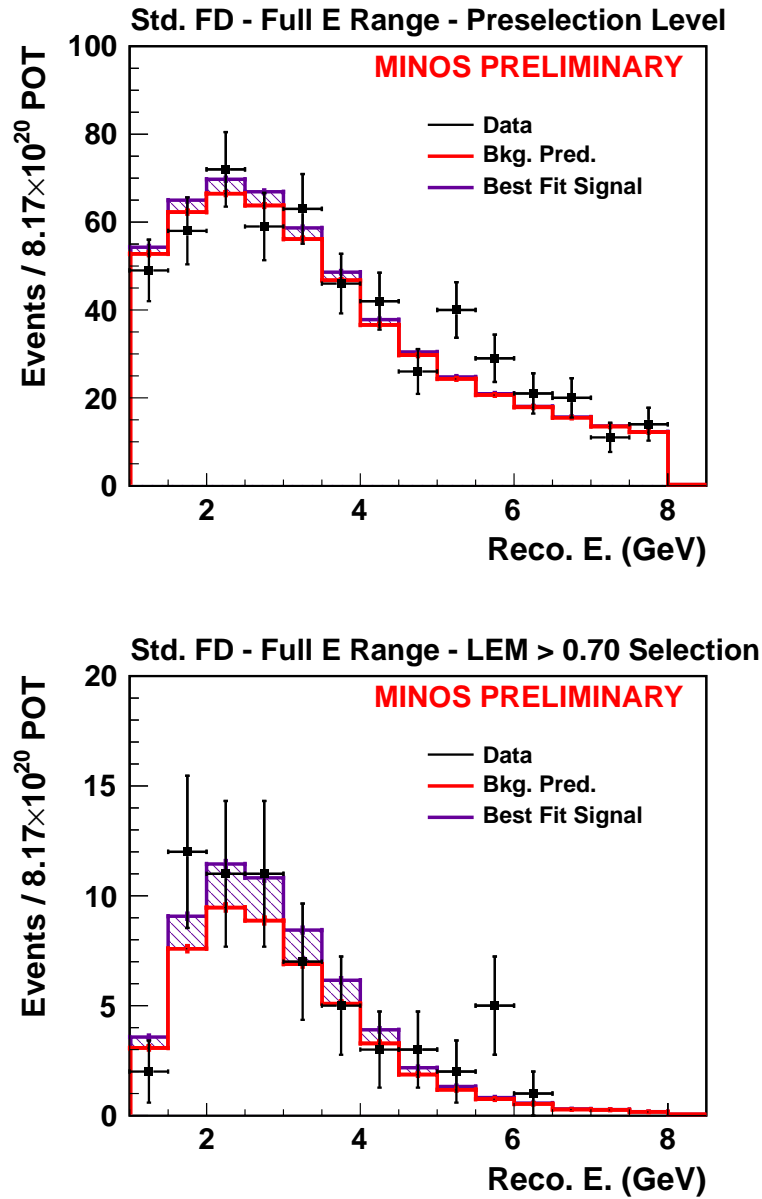


Figure 6: Reconstructed energy distribution in finer bins, of 0.5 GeV, for the Preselection (top) and LEM>0.7 (bottom), for Background Prediction (red), best fit signal (violet, at  $\sin^2(2\theta_{13}) = 0.04633$ ,  $\delta_{CP}=0$ ), and Far Data (black). Plot is for all runs and an exposure of  $8.17 \times 10^{20}$  POTs.

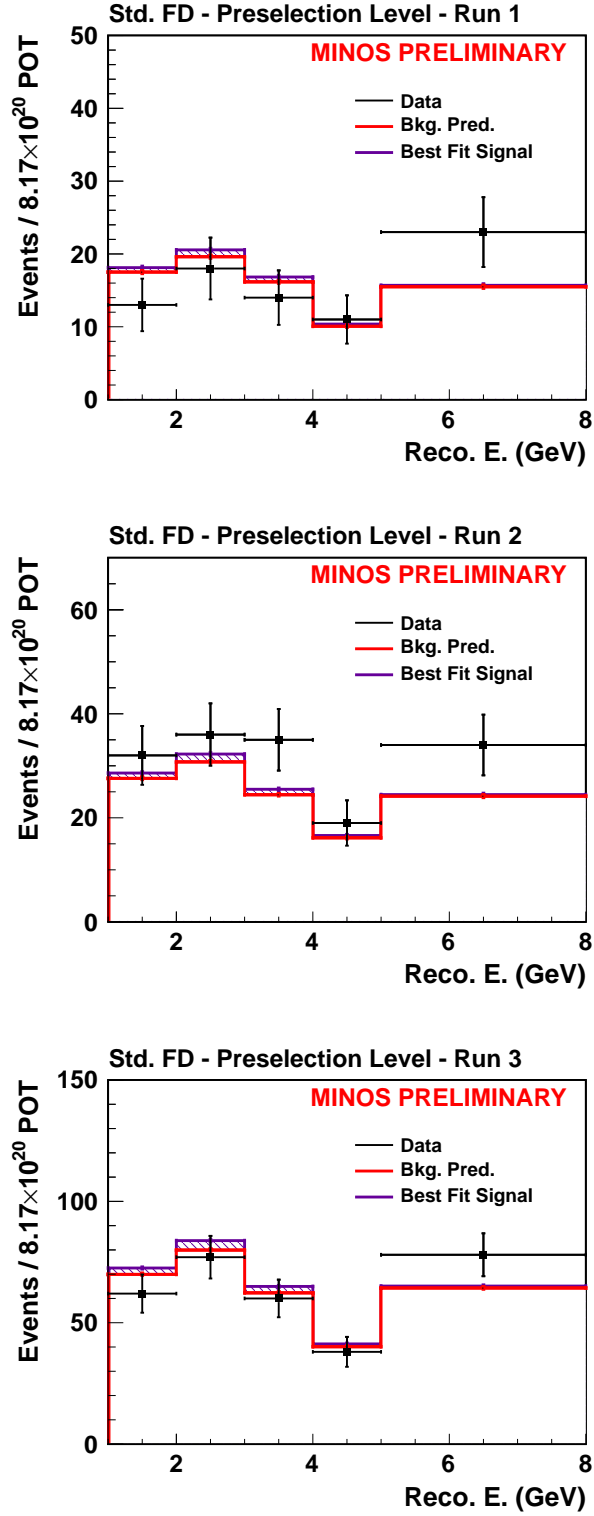


Figure 7: Preselection-level reconstructed energy distribution for Run 1 (top), Run 2 (middle), and Run 3 (bottom), for Background Prediction (red), best fit signal (violet, at  $\sin^2(2\theta_{13}) = 0.04633$ ,  $\delta_{CP}=0$ ), and Far Data (black).

### 3 Investigation of Excess at 5 GeV

Possible explanations for the 5-6 GeV excess included statistical fluctuations, a bug, or an unknown class of  $\nu_e$  CC-like events. To investigate the sample, a large number of plots were made comparing the Far Detector Data to the Prediction in various distributions (the Prediction histograms were made by reweighting the Far Detector Monte Carlo to the correct size for a given PID bin). These distributions included the LEM particle ID variables, variables describing shower and event shape (including several from the ANN11 PID), the preselection variables (track planes, track-like planes, number of showers), and numerous other basic topological and energy variables. These plots were made for events in the 1-8 GeV range ([4]), the 5-8 GeV range ([5]), and in the 5-6 GeV range ([6]). No “smoking gun” plots were found in any of these studies, indicating a class of event or a bug which could be responsible for the extra events.

In the 5-8 GeV and 5-6 GeV plot studies, one variable was possibly identified as having an anomalous distribution. This is the “RMS” variable, part of the ANN11 pid variable set. This variable as defined as the RMS of the strip hit distribution, with the distribution weighted by  $(\text{pulseheight})^2$  for each strip; only strips within 9 planes of the center and with  $>2$  pe are included in this calculation. The distributions of the RMS variable for 5-6 GeV and 5-8 GeV can be seen in Figure 8. Both distributions show a large excess in the region between  $1.6 < \text{RMS} < 2.0$ ; this exists as a large spike at 1.8-2.0 for the 5-8 GeV region, and as a wider and flatter excess in the 5-6 GeV region. While this distribution appeared promising as an explanation, most of the LEM events selected in the 5-6 GeV region have a RMS value lower than the region of this excess (see Figure 9). An RMS excess would therefore not have any effect on the  $\nu_e$ -like sample. Indeed, a visual examination of the event displays for events in the RMS spike region revealed no unusual or pathological behavior. [7] For all other variables, any interesting shape features generally disappeared when the Predicted and Data histograms were compared as area-normalized instead of POT-normalized distributions. [8] An investigation of the Far/Near Data/MC double ratios for the variables also revealed nothing. [9]

An investigation was also made of the spatial distribution of the Far Detector Data, to see if there was a pileup of events somewhere in the detector. Figure 10 shows the vertex position of events for Preselection and LEM in the XY plane, while Figure 11 shows Z position. For the Z distribution, there is some hint of a possible excess of events at the end of the second supermodule as compared to the first supermodule, as well as at the very beginning of the first supermodule; however, a lack of statistics makes it difficult to interpret this as anything except a fluctuation. Similarly, there appear to be several  $\text{LEM} > 0.7$  events in the XY distribution with vertices close to the edge of the detector. Looking at the distance of events’ vertices from the radial edge of the fiducial volume (Figure 12) reveals no large excess towards the edge of the volume. Again, there is no obvious detector-based effect or bug to explain the excess of events seen at the Preselection level.

Finally, a study was made of the preselection cuts themselves, to see if the excess appears at some specific stage in the cut process. [10] In this case, to make a prediction, the Near Data and Monte Carlo, along with the Far Monte Carlo, were processed and used to perform

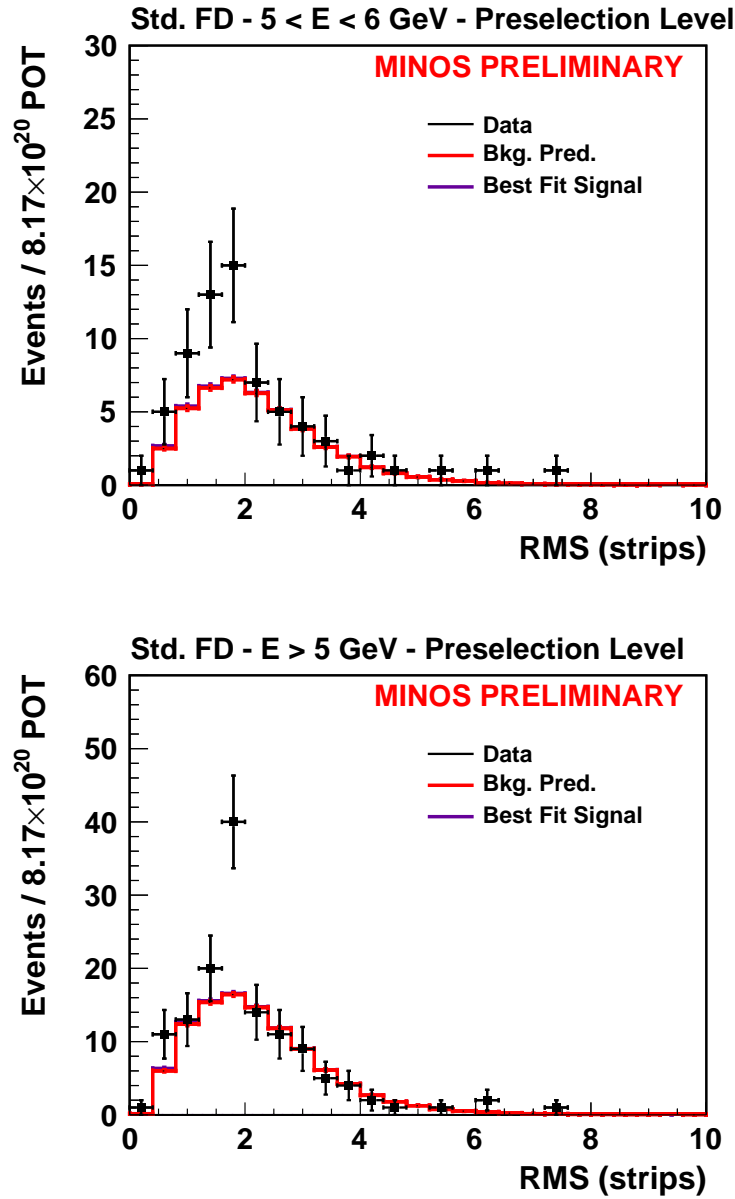


Figure 8: Preselection-level distributions for the RMS variable, for 5-6 GeV (top) and 5-8 GeV (bottom), for Background Prediction (red), best fit signal (violet, at  $\sin^2(2\theta_{13}) = 0.04633$ ,  $\delta_{CP}=0$ ), and Far Data (black). Plot is for all runs and an exposure of  $8.17 \times 10^{20}$  POTs.

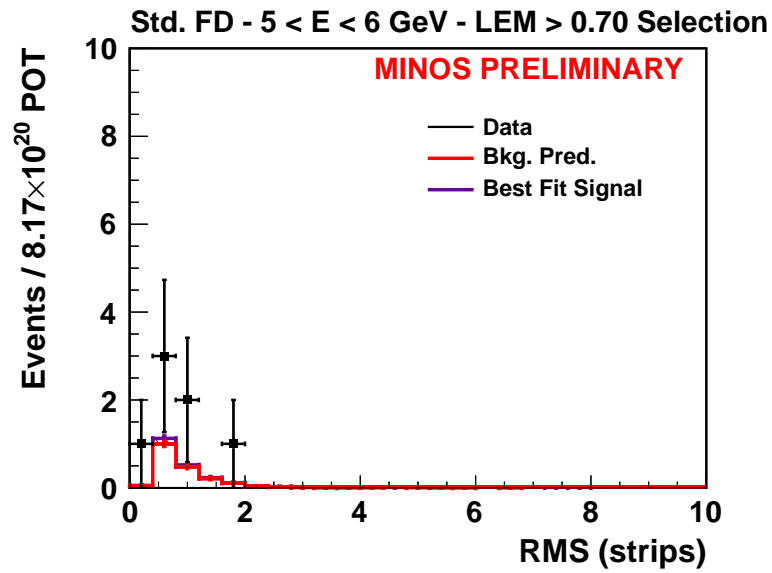


Figure 9: LEM>0.7-level distributions for the RMS variable, for 5-6 GeV, for Background Prediction (red), best fit signal (violet, at  $\sin^2(2\theta_{13}) = 0.04633$ ,  $\delta_{CP}=0$ ), and Far Data (black). 5-8 GeV is not shown, as there is only one additional event in the 5-8 GeV region for this selection. Plot is for all runs and an exposure of  $8.17 \times 10^{20}$  POTs.

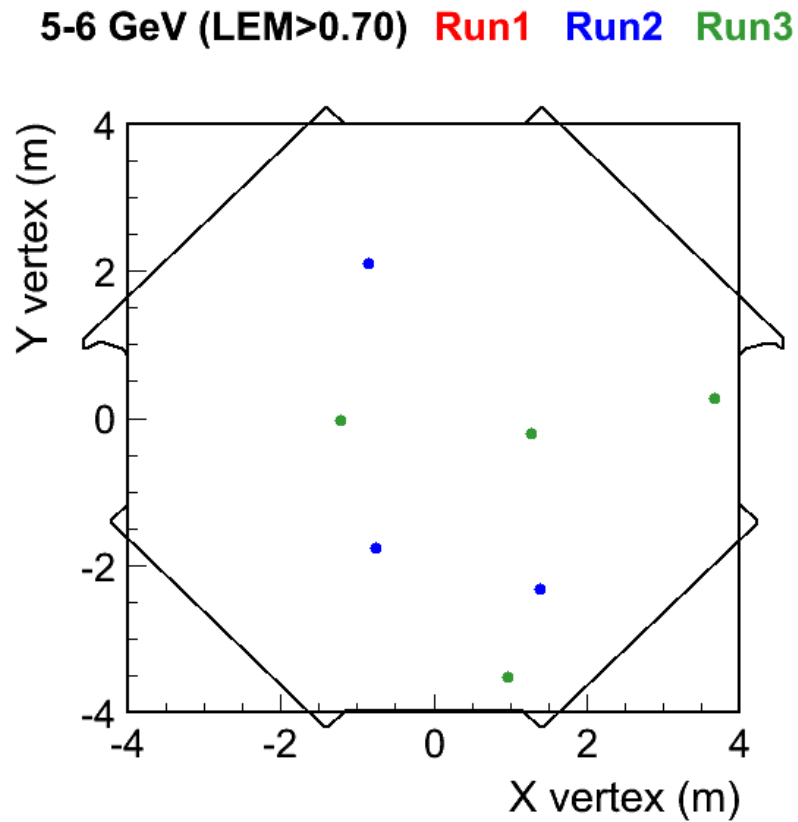
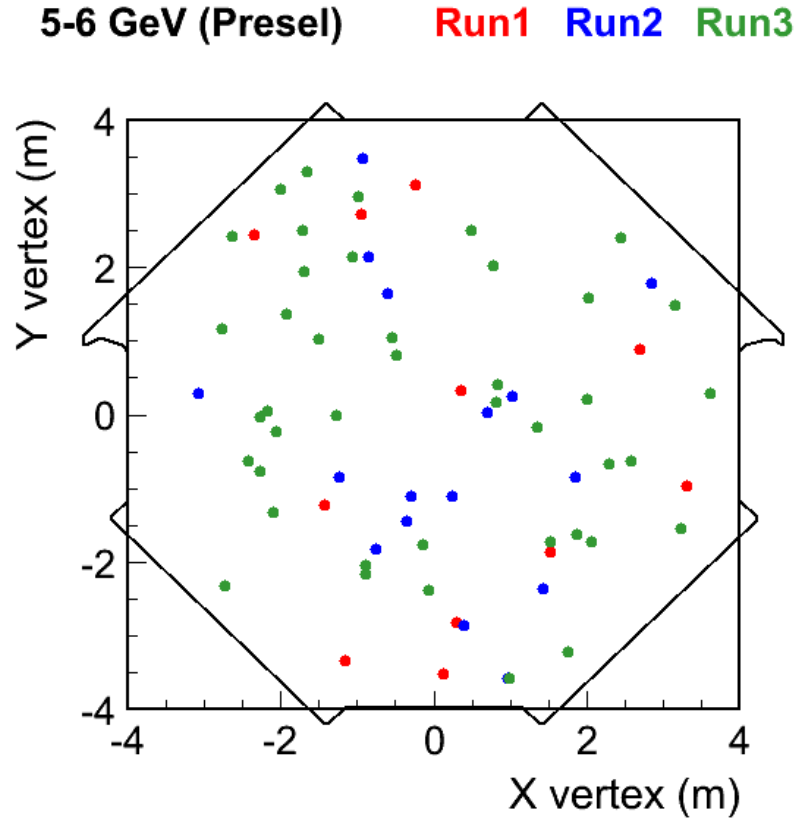


Figure 10: XY positions for Far Detector Data events in the 5-6 GeV region, for Preselection (top) and LEM>0.7 (bottom). Runs are color-coded.

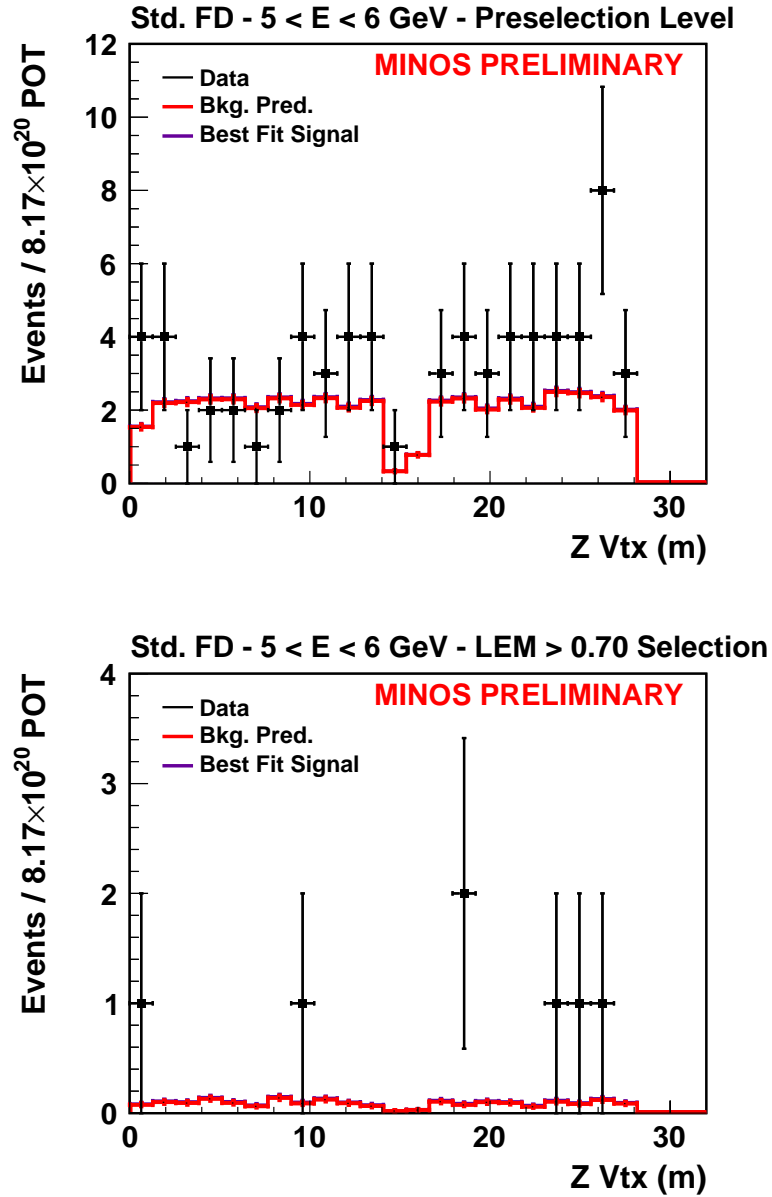


Figure 11: Z Vertex Position (m) for events in the 5-6 GeV Preselection (top) and LEM>0.7 (bottom), for Background Prediction (red), best fit signal (violet, at  $\sin^2(2\theta_{13}) = 0.04633$ ,  $\delta_{CP}=0$ ), and Far Data (black). Plot is for all runs and an exposure of  $8.17 \times 10^{20}$  POTs.

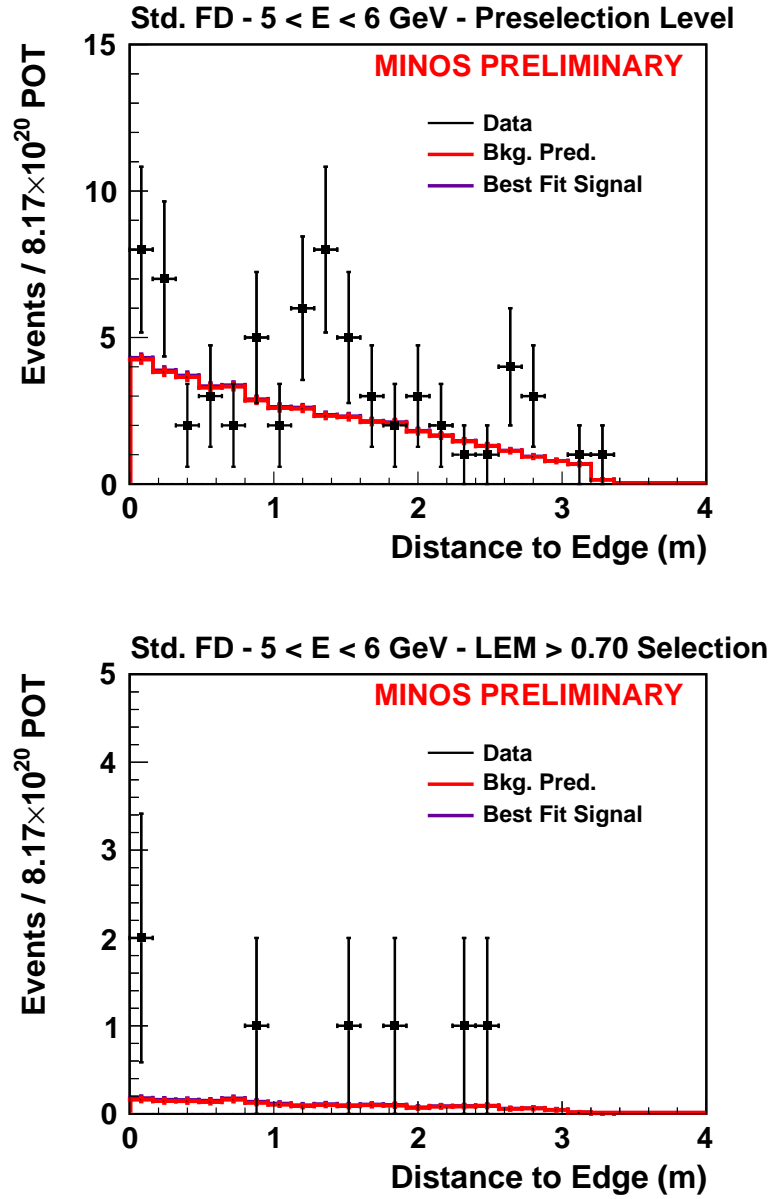


Figure 12: Distance of vertex to (radial) fiducial volume edge (m) for events in the 5-6 GeV Preselection (top) and LEM>0.7 (bottom), for Background Prediction (red), best fit signal (violet, at  $\sin^2(2\theta_{13}) = 0.04633$ ,  $\delta_{CP}=0$ ), and Far Data (black). Plot is for all runs and an exposure of  $8.17 \times 10^{20}$  POTs.

Number	Cut Description
0	Fiducial Volume Cuts, Data Quality, $1 \text{ GeV} < \text{Reco E} < 8 \text{ GeV}$
1	Cosmic Cuts
2	Is Largest Event (Far Detector)
3	Contiguous Planes $> 5$
4	Number of Showers $> 0$
5	Track Planes $< 25$
6	Track-like Planes $< 16$ (Full Preselection)

Table 2: Preselection Cut Stages. Cuts are applied successively, on top of one another.

a simple Data/MC-derived decomposition[11] in bins of PID and energy. This prediction was then compared to the data. The cuts were applied in the order found in Table 2. The resulting Data vs. Prediction reconstructed energy distributions can be seen in Figures 13 to 16. Although there are fluctuations throughout the cut sequence, the excess becomes statistically significant primarily following Preselection Cut 5, or the Track Planes cut. This suggests that the excess is primarily composed of events with smaller track lengths (or no tracks). This could pose the basis for a future exploration of the excess. Additionally, a thorough exploration of various topological variables at the stages of the preselection cut found no obvious pathologies or distribution pile-ups. [12]

As can be surmised from the above, extensive studies have been done to try to find either a bug or an analysis or physics explanation for the excess in the 5-6 GeV range, with no clear indication of a problem or statistically significant cause. References [4] to [12] should be consulted for a detailed overview of these studies.

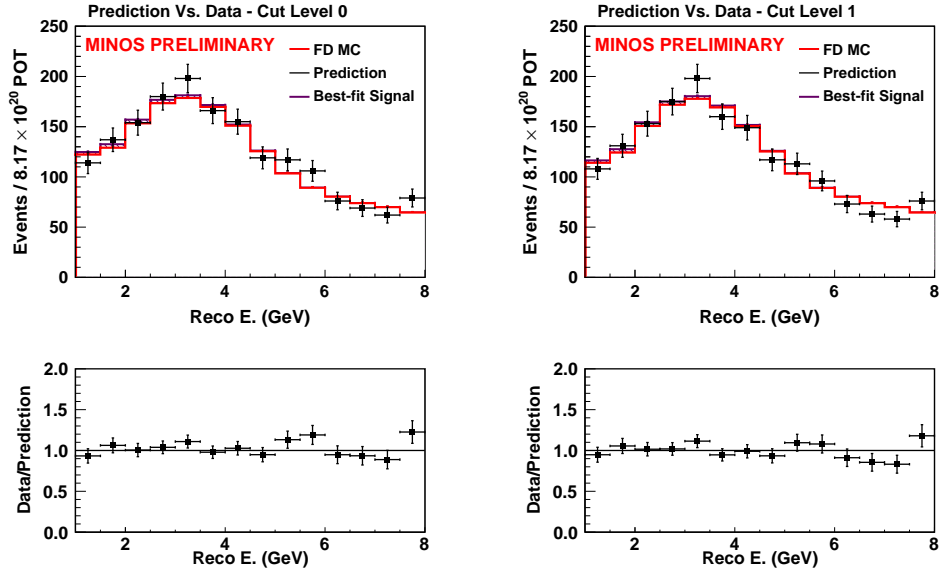


Figure 13: Reconstructed energy distribution in bins of 0.5 GeV, for Preselection Stages 0 (Fiducial, DQ, and Energy Cuts, left) and 1 (Cosmic Cuts, right), for Background Prediction (red), best fit signal (violet, at  $\sin^2(2\theta_{13}) = 0.04633$ ,  $\delta_{CP}=0$ ), and Far Data (black). Data/Prediction ratio is shown below each plot. Plot is for all runs and an exposure of  $8.17 \times 10^{20}$  POTs.

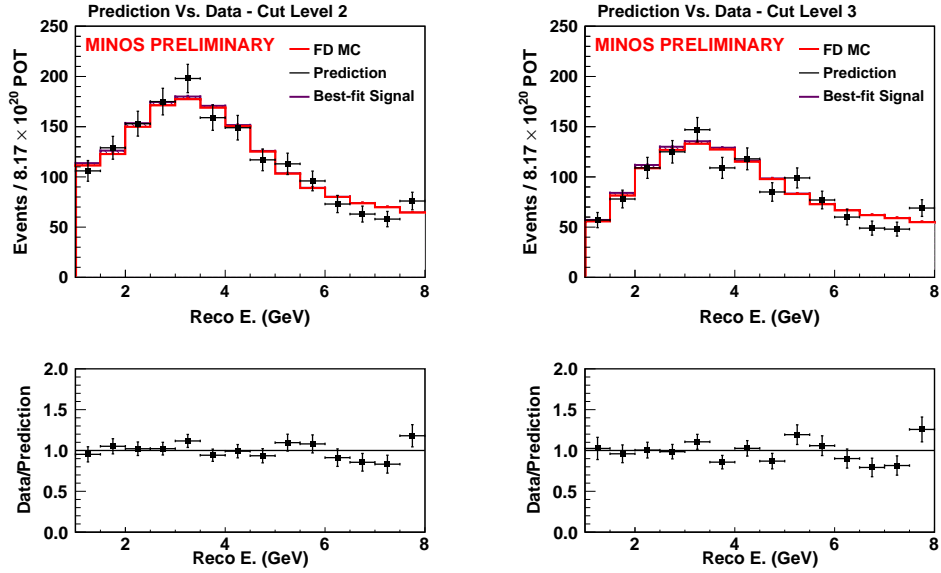


Figure 14: Reconstructed energy distribution in bins of 0.5 GeV, for Preselection Stages 2 (Is Largest Event, left) and 3 (Contiguous Planes cut, right), for Background Prediction (red), best fit signal (violet, at  $\sin^2(2\theta_{13}) = 0.04633$ ,  $\delta_{CP}=0$ ), and Far Data (black). Data/Prediction ratio is shown below each plot. Plot is for all runs and an exposure of  $8.17 \times 10^{20}$  POTs.

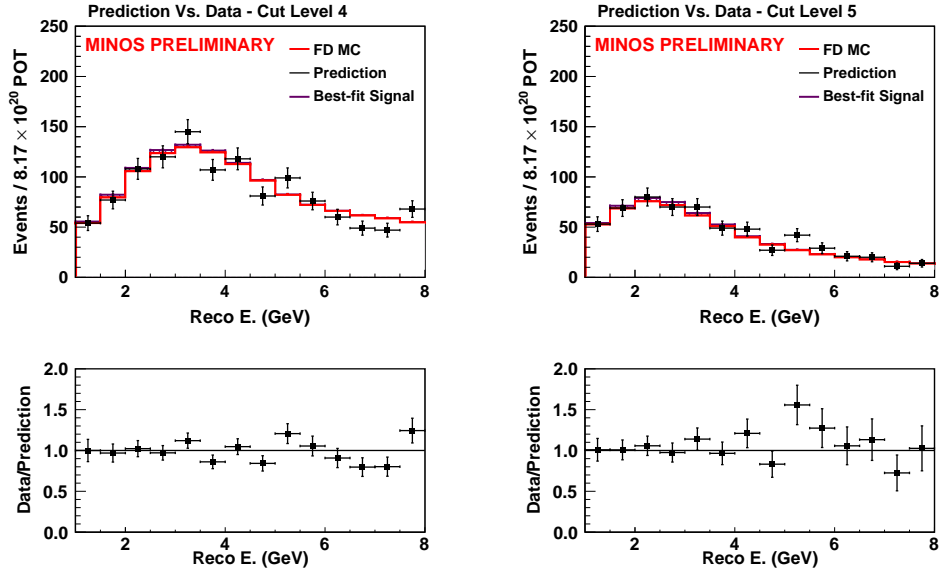


Figure 15: Reconstructed energy distribution in bins of 0.5 GeV, for Preselection Stages 4 (Number of Showers Cut, left) and 5 (Track Planes Cut, right), for Background Prediction (red), best fit signal (violet, at  $\sin^2(2\theta_{13}) = 0.04633$ ,  $\delta_{CP}=0$ ), and Far Data (black). Data/Prediction ratio is shown below each plot. Plot is for all runs and an exposure of  $8.17 \times 10^{20}$  POTs.

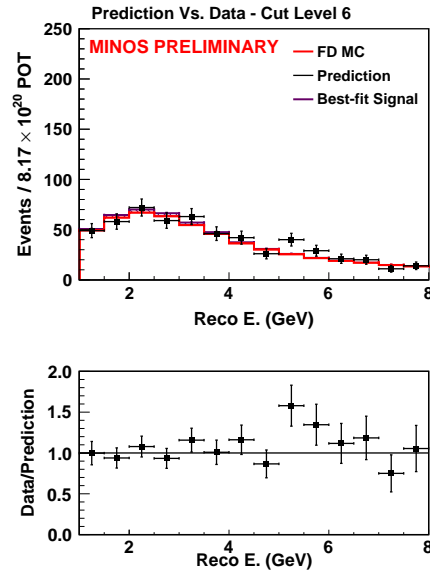


Figure 16: Reconstructed energy distribution in bins of 0.5 GeV, for Preselection Stage 6 (Track Like Planes cut, i.e. the total Preselection, left), for Background Prediction (red), best fit signal (violet, at  $\sin^2(2\theta_{13}) = 0.04633$ ,  $\delta_{CP}=0$ ), and Far Data (black). Data/Prediction ratio is shown below each plot. Plot is for all runs and an exposure of  $8.17 \times 10^{20}$  POTs.

## 4 Fitting Strategy

If we believe the 5 GeV excess is a statistical fluctuation, the analysis we’ve done is fine, because all such fluctuations are considered when calculating the Feldman-Cousins allowed region. If we knew that the excess at 5 GeV was due to some problem with the data or misunderstanding of the systematics, then removing the high energy region from the analysis would be appropriate. Unfortunately, we are in the gray area between these two scenarios. Our investigation has not turned up any obvious problems with the data, and a 2.4 sigma excess in the preselected sample could be a statistical fluctuation, but we can’t be certain.

After considerable discussions in the nue working group meetings, we have arrived at the solution of including energy information in the fit. By doing this, if the excess is in fact evidence of some problem with the data, we minimize the impact it has on our result by “fitting it out”. At the same time, we avoid cutting out data that could simply be a statistical fluctuation. Since there is little signal predicted in the 5-8 GeV bin, we expect that bin won’t have much pull on the fit and thus the allowed region obtained from the energy binned fit should be the same as that we would obtain by discarding the events above 5 GeV.

### 4.1 Energy Binning Optimization

In order to do the fit in bins of energy, we must choose an energy binning in an unbiased way. This means choosing the number of bins and the bin edges (i.e. for two energy bins, is there any reason to do 1-2, 2-8 GeV vs. 1-3, 3-8 GeV, etc.).

We repeated studies of sensitivity of various 2D LEM pid vs energy binning options (Doc-8151). The conclusions were the same as with early studies: going from one energy bin to two gives a very slight improvement in sensitivity, but all possible options for energy binning with two or more bins gives virtually identical sensitivity. Figure 17 shows the distribution of sensitivity for a number of possible options of energy binning (up to 4 bins). Each plot in the figure represents a different choice for the LEM binning. The improvement in sensitivity we achieve by using 3 LEM bins instead of 2 is evident from the mean of the distribution, while the improvement using 4 LEM bins instead of 3 is not as great. In all cases, the range of sensitivity from various options for energy binning is not large (the RMS is about 0.5% of the mean in all cases).

We also considered whether binning in energy helps to minimize the effect of statistical fluctuations. 10,000 mock data experiments were created by varying the  $\sin^2(2\theta_{13}) = 0$  prediction within its statistical and systematic uncertainties for different binning options (3 LEM bins with 1, 2, or 5 energy bins). We then looked at the 90% CL upper limit for each of these experiments. The distributions are shown in Figure 18. If binning in energy did help minimize the effect of statistical fluctuations, we would expect the distribution of possible limits to be narrower. However, there is no significant difference in these distributions.

Given that there is no compelling (quantifiable) argument to choose one energy binning over another, we settled on using the energy binning that is “natural” to the analysis. The

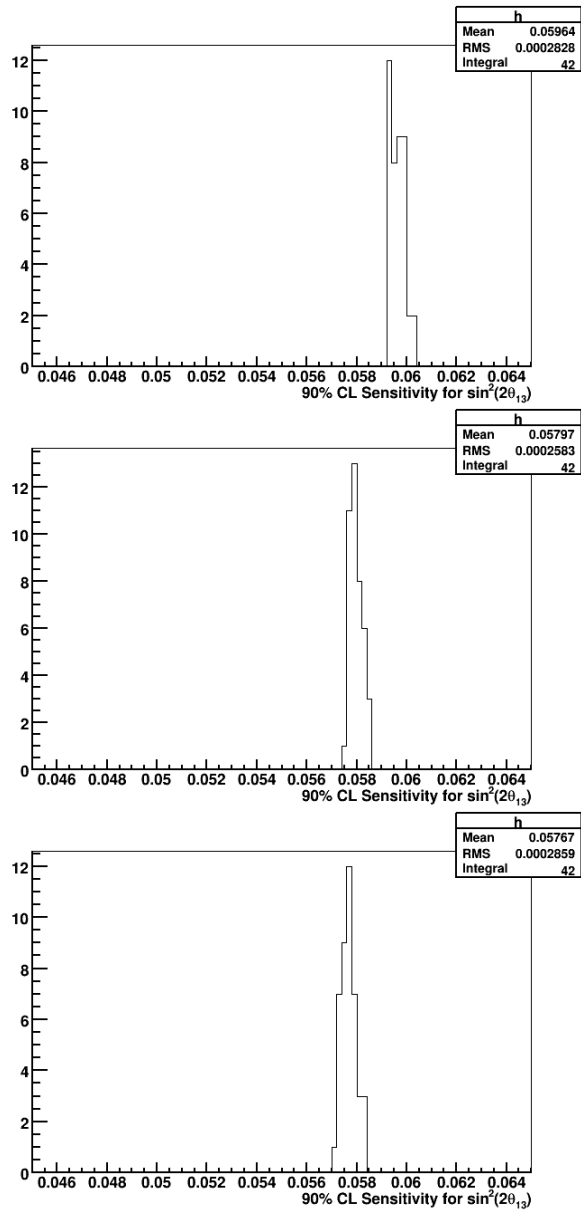


Figure 17: Distribution of sensitivity for different possible options for up to 4 energy bins, for 2 LEM bins (top), 3 LEM bins (middle), and 4 LEM bins (bottom).

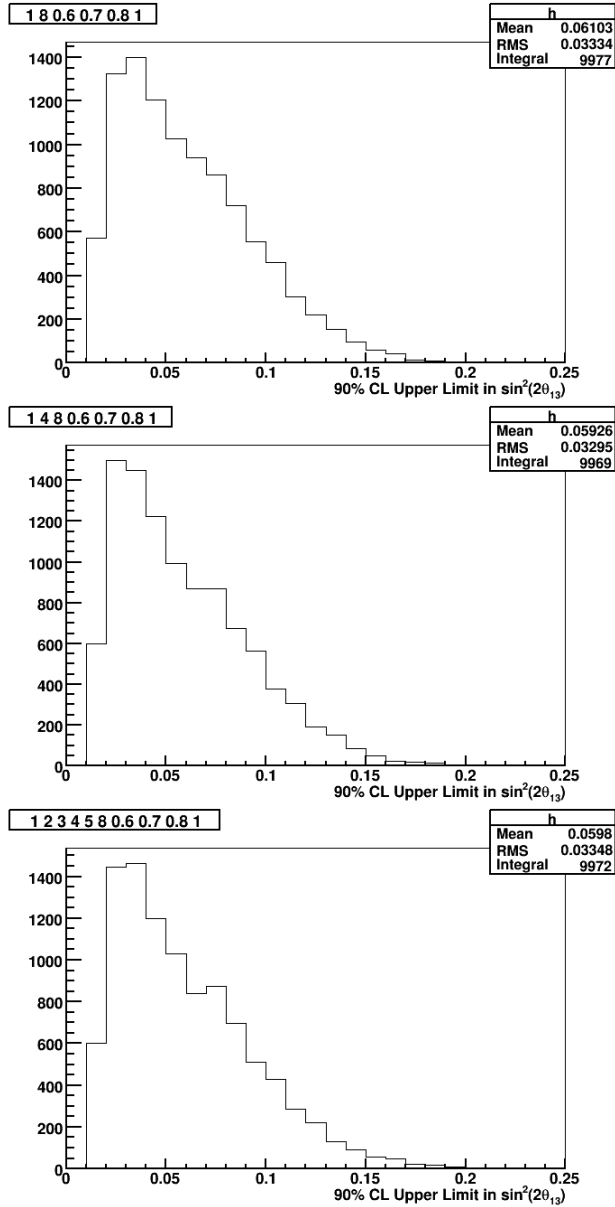


Figure 18: Distribution of possible 90% CL limits for 10,000 mock data experiments. In all cases, the fit is done with 3 LEM bins (0.6-0.7, 0.7-0.8, >0.8) and different energy binning: 1 energy bin 1-8 GeV (top), 2 energy bins 1-4, 4-8 GeV (middle), and 5 energy bins 1-2, 2-3, 3-4, 4-5, 5-8 GeV (bottom).

ND decomposition fit is done in bins of PID and energy, with 5 energy bins (1-2, 2-3, 3-4, 4-5, 5-8 GeV). We will maintain this binning throughout the analysis (ND decomposition, extrapolation to FD, and fitting). Note that we will continue to use 3 LEM bins (0.6-0.7, 0.7-0.8, >0.8), as this is still the LEM binning option that maximizes the sensitivity (gains from using 4 LEM bins are not large). Thus we will do a 15 bin fit - 3 LEM bins x 5 energy bins.

There was one technical issue that needed to be explored related to generating Feldman-Cousins contours with the new binning. The pseudo-experiments used to calculate the Feldman-Cousins contours are generated taking both systematic and statistical fluctuations into account. The likelihood function we were using to fit the pseudo-experiments uses nuisance parameters to fit the systematic fluctuations, one parameter per bin. When we increase the number of bins, we increase the number of fit parameters, causing the Minuit fit to fail more often. This means the minimum likelihood value might not be correct in all cases, possibly biasing our results.

However, since we take systematics into account when generating the pseudo-experiments, we may not need to also fit the systematic nuisance parameters. In the Feldman-Cousins method, the likelihood value is only used to rank the experiments in order of best fit to worst, so as long as the likelihood value is calculated the same way for each pseudo-experiment and that ranking is the same, the actual value of the likelihood doesn't matter. We investigated this by calculating the Feldman-Cousins contours at  $\delta = 0$  for the 3 bin LEM (1 energy bin) fit to the real data for two cases: 1) fitting the nuisance parameters for each pseudo-experiment or 2) using the simple likelihood with no nuisance parameters. The result is shown in Figure 19. The curves are basically identical for the two cases, and so we conclude that we can correctly calculate the Feldman-Cousins contours for our 15 bin fit without fitting for the nuisance parameters.

## 5 Summary

## References

- [1] R. Patterson, MINOS-doc-7997, 2011.
- [2] L. Whitehead, MINOS-doc-8135, 2011.
- [3] L. Whitehead, R. Toner, M. Orchanian, MINOS-doc-8151, 2011
- [4] J. Nelson et al., MINOS-doc-8092-v2, 2011.
- [5] R. Toner, MINOS-doc-8131-v1, 2011.
- [6] R. Toner, MINOS-doc-8157-v2, 2011.
- [7] R. Patterson, MINOS-doc-8093-v1, 2011.

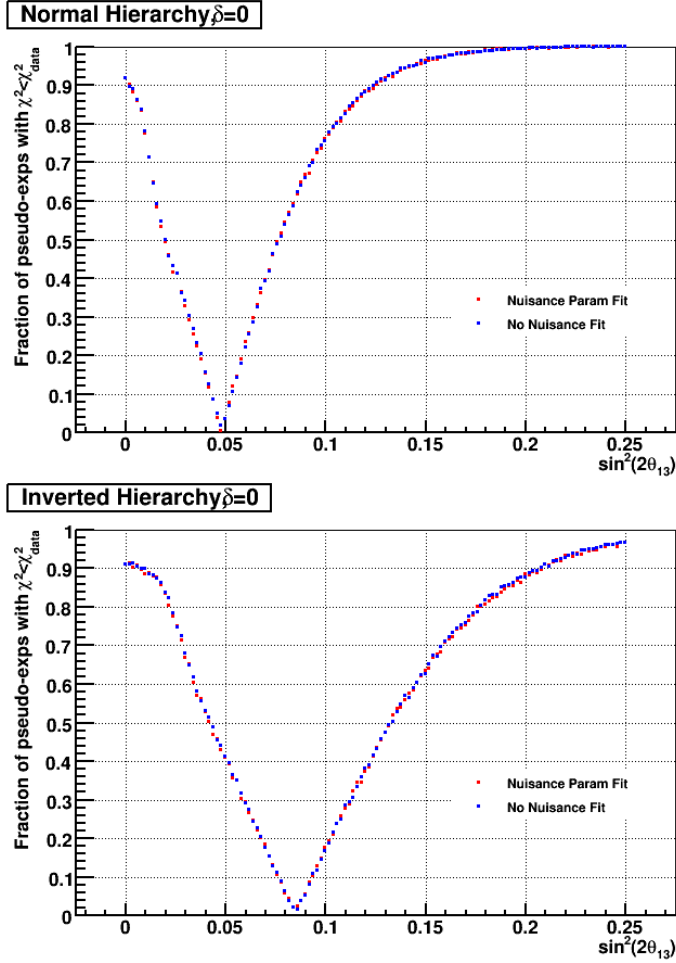


Figure 19: These curves represent the FC contours for  $\delta = 0$  for the 3 bin LEM fit to the actual data. The 90% CL limits for  $\sin^2(2\theta_{13})$  are the values of  $\sin^2(2\theta_{13})$  where the curves cross  $y=0.9$ . The best fit value of  $\sin^2(2\theta_{13})$  is the value at the minimum of the curves. Top: Normal mass hierarchy, Bottom: Inverted mass hierarchy

- [8] R. Toner, MINOS-doc-8165-v1, 2011.
- [9] R. Toner, MINOS-doc-8128-v2, 2011.
- [10] R. Toner, MINOS-doc-8166-v1, 2011.
- [11] P. Ochoa, R. Patterson, MINOS-doc-3760-v1, 2007.
- [12] T. Vahle, MINOS-doc-8181-v2, 2011.